Published in final edited form as:
ACS Biomater Sci Eng. 2019 December 09; 5(12): 6511–6519. doi:10.1021/acsbiomaterials.9b01178.

Fabrication and Characterization of Pectin Hydrogel Nanofiber Scaffolds for Differentiation of Mesenchymal Stem Cells into Vascular Cells

Na Li[†], **Fuxin Xue**[‡], **Hui Zhang**[‡], **Hanna J. Sanyour**[†], **Alex P. Rickel**[†], **Andrew Uttecht**[†], **Betty Fanta**[†,§], **Junli Hu**[*,‡], **Zhongkui Hong**[*,†,§]

[†]Department of Biomedical Engineering, University of South Dakota, Sioux Falls, South Dakota 57107, United States

[‡]Key Laboratory of UV-Emitting Materials and Technology (Northeast Normal University), Ministry of Education, Changchun, Jilin 130024, P. R. China

[§]BioSNTR, Sioux Falls, South Dakota 57107, United States

Abstract

Despite significant progress over the past few decades, creating a tissue-engineered vascular graft with replicated functions of native blood vessels remains a challenge due to the mismatch in mechanical properties, low biological function, and rapid occlusion caused by restenosis of small diameter vessel grafts (<6 mm diameter). A scaffold with similar mechanical properties and biocompatibility to the host tissue is ideally needed for the attachment and proliferation of cells to support the building of engineered tissue. In this study, pectin hydrogel nanofiber scaffolds with two different oxidation degrees (25 and 50%) were prepared by a multistep methodology including periodate oxidation, electrospinning, and adipic acid dihydrazide crosslinking. Scanning electron microscopy (SEM) images showed that the obtained pectin nanofiber mats have a nano-sized fibrous structure with 300–400 nm fiber diameter. Physicochemical property testing using Fourier transform infrared (FTIR) spectra, atomic force microscopy (AFM) nanoindentations, and contact angle measurements demonstrated that the stiffness and hydrophobicity of the fiber mat could be manipulated by adjusting the oxidation and crosslinking levels of the pectin hydrogels. Live/Dead staining showed high viability of the mesenchymal stem cells (MSCs) cultured on the pectin hydrogel fiber scaffold for 14 days. In addition, the potential application of pectin hydrogel nanofiber scaffolds of different stiffness in stem cell differentiation into vascular cells was assessed by gene expression analysis. Real-time polymerase chain reaction (RT-PCR) results showed that the stiffer scaffold facilitated the differentiation of MSCs into vascular smooth muscle cells, while the softer fiber mat promoted MSC differentiation into endothelial cells. Altogether, our results indicate that the pectin hydrogel nanofibers have the capability of providing mechanical

[*]**Corresponding Authors**: hujl100@nenu.edu.cn (J.H.). Zhongkui.Hong@usd.edu (Z.H.).

Author Contributions

N.L. and F.X. contributed equally. All authors have given approval to the final version of the manuscript.

Supporting Information

The Supporting Information is available free of charge on the ACS Publications website at DOI: 10.1021/acsbiomaterials.9b01178.

OCP25-ADH nanofiber mat after incubation in SBF for 10 and 14 days (Figure S1) (PDF)

The authors declare no competing financial interest.

cues that induce MSC differentiation into vascular cells and can be potentially applied in stem cell-based tissue engineering.

Graphical Abstract

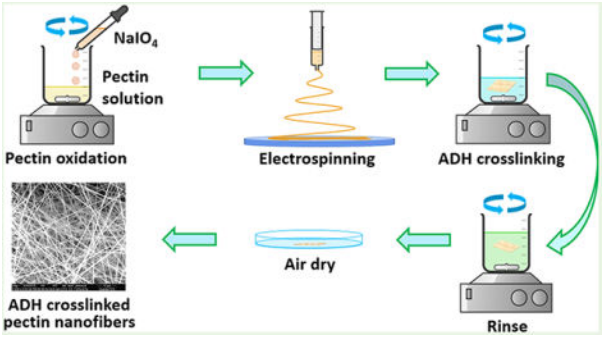

Keywords

electrospin; pectin; hydrogel; scaffold; mesenchymal stem cell; vascular cells

1. INTRODUCTION

Although significant progress has been made, creating tissue-engineered vascular grafts with replicated mechanical properties and biological functions of native blood vessels remains challenging.[1–4] Native blood vessels are composed of a single layer of endothelial cells (ECs) on the luminal surface and multiple layers of vascular smooth muscle cells (VSMCs) embedded in a fibrous extracellular matrix (ECM) in the middle layer of the blood vessel wall.[5] A scaffold with similar mechanical properties and biocompatibility to the natural blood vessel wall is ideally needed for cell attachment and proliferation to support vessel graft formation. At present, the major sources of fibrous vessel scaffolds are decellularized vascular ECM scaffolds[6–8] and electrospun polymer nanofiber scaffolds.[9,10] Both scaffolds have their respective advantages and limitations when applied in vascular tissue engineering.[5,9–12] Decellularized ECM scaffolds provide not only excellent mechanical strength and biocompatibility, but also beneficial bioactive components for cell growth and stem cell differentiation in tissue engineering and regenerative medicine.[13–15] Challenges of using decellularized ECM scaffolds, however, include the potential risk of infection and disease transmission, and potential host immune rejection to the cellular debris retained in the ECM scaffolds during the decellularization process.[11,12,16] Compared to the native decellularized ECM scaffolds, synthetic scaffolds are of low cost and can avoid donor site injury, which frequently creates additional wound and pain for the donor and/or at-risk patient.[10] However, similar to acellular synthetic grafts, low biological function limits the application of the synthetic scaffolds in vascular tissue engineering.[17,18]

An ideal scaffold should have specific physicochemical and physiological properties similar to native tissue (i.e., mechanical strength and biological functions) to provide sufficient binding sites for cellular growth, proliferation, ECM secretion, and tissue formation.[19–23] Electrospinning has been reported as a powerful technique for creating biomimetic

scaffolds with nanoscale fibrous structures similar to native ECM proteins.[24,25] The mechanical properties of polymeric fibrous scaffolds can be potentially tuned by varying the composition of the polymer solution to provide appropriate mechanical properties and surface characteristics, which may guide cellular responses and determine cell fate in tissue engineering.[10,26,27] Pectin is a heteropolysaccharide obtained from sunflower heads and citrus fruits and is mainly composed of partially esterified/amidated galacturonic acid (GalA) residues.[28] As researchers continue to discover the potential therapeutic advantages of pectin, e.g., antitumor and anti-inflammation effects, there has been growing interest in the application of pectin in the biomedical field.[29–31] Multiple pectin formulations, including hydrogels, films, nanoparticles, and nanofiber mats, have been developed for biomedical applications,[32–34] such as drug delivery,[35] tissue engineering,[36] and wound healing.[37]

The EC layer provides multiple antithrombogenic functions for native blood vessels; the lack of EC lining on the vessel graft lumen is considered a major problem that could potentially cause poor patency of the resulting engineered vessel grafts.[4,38–40] In our previous study, EC-like cells obtained by the on-site differentiation of mesenchymal stem cells (MSCs) on decellularized ECM scaffolds demonstrated that it could potentially overcome this drawback in engineered vessel grafts.[7] The capability of decellularized carotid vessel scaffold in facilitating MSC–VSMC differentiation has also been reported previously.[13] The underlying mechanism by which the decellularized ECM scaffold promotes MSC-vascular cell differentiation may lie in the bioactive component proteins in the ECM, such as laminin, fibronectin, vitronectin, collagen, and gelatin, among others.[41–43] Additionally, an ideal mechanical support provided by each side of the native vascular ECM (soft in the lumen side and stiff in the adventitial side) might be another reasonable interpretation for the inductive effect on MSC differentiation exerted by the ECM. A similar finding was reported by Wingate et al. that lineage commitment of MSCs toward specific vascular cells could be controlled by carefully designing the substrate modulus.[44] However, in terms of the underlying mechanism, how mechanical cues regulate the differentiation of MSCs into vascular cells is still not fully understood.

In this study, we aimed to fabricate adipic acid dihydrazide (ADH)-crosslinked pectin hydrogel into a nanofiber mat to replicate the mechanical properties and fibrous architecture of the natural blood vessel wall ECM using electrospinning technology. The biocompatibility and potential application of the obtained pectin fiber mats with different mechanical properties were assessed by culturing MSCs on the pectin hydrogel fiber scaffolds and inducing them to differentiate into VSMCs and ECs.

2. MATERIALS AND METHODS

2.1. Materials.

Pectin from citrus peel (CP, degree of esterification = 70.2%) was supplied by Sigma-Aldrich (Shanghai, China). Adipic acid dihydrazide (ADH), hydroxylamine hydrochloride, methyl orange, and poly(ethylene oxide) (PEO, M_v = 5000 kDa) were purchased from Aladdin Reagents (Shanghai, China). Triton X-100 was supplied by Dingguo Biotech

(Beijing, China). Sodium periodate ($NaIO_4$) and dimethyl sulfoxide (DMSO) were obtained from Xilong Chemicals (Guangzhou, China).

2.2. Synthesis of Oxidized Pectins (OCPs).

Pectin solution (5% w/w) was prepared by dissolving pectin with water overnight and then mixed with $NaIO_4$ solution in water. The final concentration of pectin in the reaction solution was 2% (w/w). The molar ratios between $NaIO_4$ and galacturonic acid units (GalA) of pectin were set at 30:100 and 50:100, respectively. After being stirred in the dark at ambient temperature (25 °C) for 16 h, the solutions were transferred to dialysis tubes with a cutoff molecular weight of 3.5 kDa and dialyzed against a large amount of water. The purified solutions were then lyophilized to obtain oxidized pectins (OCPs). The content of the aldehyde groups, degree of oxidation, and molecular weight of OCPs were determined as described in our previous work.[34,45]

2.3. Electrospinning of OCPs.

PEO, a flexible polymer, was used to enhance molecular chain entanglements of OCPs and facilitate the production of OCP nanofibers using electrospinning.[46] Solutions of OCP (2% w/w) and PEO (5% w/w) were prepared separately by dissolving the polymers with water. The OCP solutions were then mixed with the PEO solution. The mass ratio between OCP and PEO was 80:20. Triton X-100, dimethyl sulfoxide, and water were then added to the mixtures to reach a final concentration of Triton X-100 and dimethyl sulfoxide of 1 and 5% w/w, respectively. The mixed solutions were stirred for 2 days and then fed into a 5 mL disposable syringe capped with a 9-gauge stainless-steel needle. A DC voltage of 9 kV (High DC power supply, Dalian Dingtong Technology, China) was applied between the syringe tip and a grounded flat collector covered with an aluminum foil. The distance between the syringe tip and the grounded flat collector was 15 cm. All electrospinnings were carried out at a temperature of around 30 °C and humidity of around 30%.

2.4. Crosslinking of the Electrospun OCP Nanofibers with Adipic Acid Dihydrazide (ADH).

ADH solution was prepared by dissolving ADH in water and followed by mixing with ethanol to reach an ADH concentration of 50 mM and a volume content of ethanol of 80%. OCP nanofibers (5 mg) were placed into the ADH solutions (5 mL). The mixtures were then shaken at 100 rpm for 8 h at room temperature. The crosslinked nanofibers were washed with a large amount of water to remove the excess ADH and PEO as well, rinsed with ethanol, and dried with chloroform.

2.5. Composition Characterization.

The Fourier transform infrared (FTIR) spectra were collected with an FTIR spectrometer (iS10, Thermo Scientific Nicolet) equipped with a photomultiplier detector. The samples were homogeneously mixed with KBr at a weight ratio of 1:80 and pressed into pellets. Spectra were obtained by recording 48 scans between 2000 and 800 cm^{-1} with a resolution of 4 cm^{-1}.

2.6. Morphology Observations.

The morphologies of the nanofibers were observed through a scanning electron microscope (SEM, XL-30 ESEM FEG, Micro FEI Philips) at an acceleration voltage of 20 kV. The samples were attached to sample stages with conductive tapes and sputter-coated with a thin layer of gold before measurements.

2.7. Water Wettability.

To visualize the wettability of the pectin hydrogel nanofiber scaffolds, a 2 μL drop of deionized water was dropped onto each scaffold through a micropipette needle. Videos were recorded until the drop was completely absorbed by the scaffolds with a contact angle measuring instrument (Drop Shape Analyzer, KRUSS, DSA100).

2.8. Degradation.

The pectin hydrogel nanofiber scaffolds (10 mg) were incubated in simulated body fluid (SBF, 10 mL) at 37 °C. At certain time points, the scaffolds were taken out, washed with distilled water six times to remove the remaining inorganic salts in the nanofiber scaffolds, rinsed with ethanol and chloroform, and then air dried for 24 h. The morphologies of the samples were observed by SEM (XL-30 ESEM FEG, Micro FEI Philips). The mass was weighed with an analytical balance with a readability of 0.01 mg (Mettler Toledo XSE). Three samples were tested in parallel.

Scaffold degradation under cell culture conditions was also monitored by incubating scaffolds in MSC culture medium (ATCC) supplemented with an MSC growth kit (ATCC) at 37 °C. Scaffolds were imaged at various time points by a dissection microscope (Olympus, SZX10) with an Olympus DP22 Digital Camera.

2.9. Stiffness Measurement Using Atomic Force Microscopy.

Scaffolds were incubated in complete MSC medium at 37 °C and stiffness was measured at various time points. The atomic force microscope (AFM, model: MFP-3D BIO, Asylum Research, Santa Barbara, CA) mounted on an inverted microscope (model: IX73, Olympus America Inc) was used to quantify the elastic modulus. A 5 μm glass sphere attached to a silicon nitride tip (0.03 N/m) (MLCT-O10, Bruker, Santa Barbara, CA) was used to probe the material surface at an indentation speed of 2 μm/s. At least five different spots per sample material for three different samples were measured. The Young's modulus was estimated by fitting a modified Hertz model onto the AFM indentation curve using the built-in function of the AFM software (Asylum Research).[47,48]

2.10. Cell Maintenance Culture and Differentiation.

Human bone marrow derived MSCs were cultured in MSC medium (ATCC) supplemented with the MSC growth kit (ATCC). MSCs were subcultured when the cell density reached 90% confluence and the medium was refreshed every 2 days.

To evaluate the effect of two different nanofiber scaffolds on the differentiation of MSCs into VSMCs, MSCs were seeded on different scaffolds in a 24-well plate (Corning) with a final concentration of 4×10^4 cells/well and cultured in complete MSC medium

supplemented with 10 ng/mL transforming growth factor-β1 (TGFβ1, Invitrogen) for 14 days. The differentiation of MSCs into ECs was also studied as a similar strategy described above. MSCs were seeded on different scaffolds in a 24-well plate (Corning) with a final concentration of 2×10^4 cells/well and cultured in complete EC medium (ATCC) supplemented with 50 ng/mL vascular endothelial growth factor (VEGF, Invitrogen) for 14 days.

2.11. Cell Viability Measurement.

To evaluate VSMC-like or EC-like cell viability in different nanofiber scaffolds, fiber mats with cells attached on and cultured for 14 days were incubated with calcein-AM/ethidium homodimer (EthD-1) solution (Invitrogen) at 37 °C for 1.5 h. After being washed twice with phosphate-buffered saline (PBS), the fiber samples were then examined using a confocal laser scanning microscope (IX83 FV1200, Olympus). Only live cells were distinguished by the presence of ubiquitous intracellular esterase activity that can digest nonfluorescent calcein-AM into fluorescent calcein emitting green fluorescence, whereas dead cells with damaged membranes allow the entrance of EthD-1 that produces bright red fluorescence upon binding to nucleic acids.

2.12. Real-Time Quantitative Polymerase Chain Reaction (qRT-PCR) Analysis.

For gene expression analysis with real-time RT-PCR, total cellular RNA from the constructs cultured for 14 days was extracted using TRIzol reagent (Invitrogen) following supplier's instructions and total RNA concentration was determined by spectrophotometric analysis at 260 nm. A portion of 200 ng of RNA was subjected to reverse transcription in a 20 μL reaction mixture using a High Capacity cDNA Reverse Transcript kit (Applied Biosystems, Forster City, CA). Real-time PCR was performed with Taqman gene expression assays (Applied Biosystems) through an Applied Biosystems 7500 Fast Real-Time PCR instrument. The relative mRNA expression level for α-actin (Hs00426835), calponin (Hs00206044), smoothelin (Hs00199489), CD31 (Hs01065279), von Willebrand factor (vWF, Hs01109446), and fetal liver kinase-1 (Flk-1, Hs00911700) were normalized to β-actin (Hs01060665). Each sample was analyzed in triplicate.

3. RESULTS AND DISCUSSION

3.1. Preparation of Pectin Hydrogel Nanofiber Scaffolds.

Pectin hydrogel nanofiber scaffolds were prepared by a multistep methodology including periodate oxidation, electrospinning, and ADH crosslinking (Figure 1a). Pectin was first oxidized by $NaIO_4$ to form dialdehyde groups on its molecular chains. Hydroxylamine hydrochloride titration results showed that at $NaIO_4$/GalA molar ratios of 30:100 and 50:100, the oxidation degrees of pectin are 25 and 50%, respectively. The chemical structure of the obtained pectin hydrogel nanofiber scaffolds is illustrated in Figure 1b. These results indicate that the periodate oxidation of pectin is highly efficient. FTIR results confirmed the formation of aldehyde groups in oxidized pectins (OCPs). Pristine pectin showed infrared absorbance at 1630 and 1740 cm^{-1}, which were assigned to the C=O stretching of the carboxylate and methyl ester groups, respectively (Figure 1c). OCP25 and OCP50 show significantly decreased absorbance at 1740 cm^{-1} and increased absorbance at 1630 cm^{-1},

suggesting that some ester groups of pectin were hydrolyzed into carboxylate during the process of oxidation. The hydrolysis of ester groups of pectin in aqueous conditions was observed in our previous study.[49] The aldehyde groups in OCPs were attributed to the absorbance at 1740 cm^{-1}, which was compromised by the hydrolysis of ester. In addition, OCPs exhibited a remarkable increase in the absorbance at 1100 cm^{-1}, possibly due to some aldehyde groups generated by periodate oxidation reacted with adjacent hydroxyl groups in sugar rings to form acetals or hemiacetals in the solid state for FTIR measurement. We also observed higher absorbance at 1740 and 1100 cm^{-1} from the spectrum of OCP50 than that of OCP25 due to more aldehyde groups in OCP50.

OCPs were readily electrospun into smooth nanofibers of uniform size (Figure 2a, the as-spun OCP25 and OCP50 nanofibers). The degree of oxidation seems to have little effect on the size and morphology of the nanofibers. The OCP nanofibers were then crosslinked with ADH. The nanofibrous morphology of the OCP nanofibers was not changed by ADH crosslinking (Figure 2a, ADH-crosslinked OCP25 and OCP50 nanofibers). The size of the nanofibers seemed slightly greater than the as-spun ones but remained uniform. In comparison with OCPs, the crosslinked OCP nanofibers (Figure 1, OCP25-ADH and OCP50-ADH) showed significantly decreased infrared absorbance at 1740 and 1100 cm^{-1}, as well as new absorbance at 1670 and 1550 cm^{-1}. These results confirmed that ADH reacted with aldehyde groups of OCP, forming dihydrazone crosslinkers between pectin chains. The water wettability of pectin nanofiber mats was tested using contact angle measurements. When water drop contacted pectin hydrogel nanofiber scaffolds, OCP25-ADH exhibited a contact angle of 26° and absorbed the water drop completely in 1 s. In contrast, OCP50-ADH exhibited a contact angle of 50° and took 2 s to absorb the water drop completely (Figure 2b). These results indicate that OCP50-ADH has a relatively lower water wettability than OCP25-ADH, because the crosslinking reagent ADH has hydrophobic alkyl units and more hydrophobic units are incorporated into the pectin hydrogel nanofiber scaffold at a higher oxidation degree.

3.2. Stiffness and Degradation Properties of the Pectin Hydrogel Nanofiber Scaffolds.

The pectin hydrogel nanofiber scaffolds lost their mass almost linearly in SBF (Figure 3a). The OCP25-ADH nanofiber scaffold degraded completely in 10 days, while OCP50-ADH still retained 27% of their initial mass after 14 days. It should be noted that the OCP25-ADH nanofiber scaffolds demonstrated no significant morphological changes after 10 days incubation in SBF but completely dissolved after washing with distilled water four to five times (Figure S1). Pectin hydrogel is much more unstable in pure water than the cell culture medium and buffer solution such as SBF and PBS. Therefore, part of the weight loss in this degradation experiment resulted from exhaustive washing with distilled water. The nanofibrous morphology of the scaffolds was retained during the process of degradation (Figure 3b). These results demonstrated that the ADH-crosslinked nanofiber scaffolds were degradable, and they could retain the nanofibrous feature during degradation and mass loss, which would potentially benefit cell attachment and proliferation on the nanofiber scaffolds in tissue engineering. The slower degradation rate for the OCP50-ADH with a higher oxidation degree was mainly due to the higher crosslinking density.

To examine the degradation behavior of pectin nanofiber scaffolds in the MSC culture medium, a parallel study was conducted by monitoring the changes in the morphology and stiffness of pectin nanofiber scaffolds incubated in MSC culture medium at 37 °C. After incubation in complete MSC medium, no obvious degradation was observed for both ADH-crosslinked nanofiber scaffolds after 14 days (Figure 4a). This indicates that the slow degradation of scaffolds in MSC culture medium would have no significant effect on cell proliferation and differentiation during the 14 days experiments. The *E*-moduli of nanofiber mats were tested using AFM at different time points over 14 days of incubation. OCP25-ADH pectin hydrogel nanofibers demonstrated a relative low *E*-modulus compared to the OCP50-ADH nanofibers (Figure 4b). The higher stiffness of the OCP50-ADH nanofibers resulted from its higher oxidation degree and thus the higher crosslinking density. The *E*-moduli of OCP25-ADH nanofiber scaffolds started to decrease after 10 days incubation, while no obvious decrease in *E*-moduli of OCP50-ADH scaffolds was observed after 14 days.

3.3. Cell Viability of VSMC-like Cells and EC-like Cells.

High cell viability is a crucial requirement for MSC differentiation.[50] Live/Dead staining (calcein-AM/EthD-1 staining) was applied to evaluate MSC viability during differentiation of MSCs into VSMCs or ECs in the current study. As shown in Figure 5, both VSMC-like cells and ECs-like cells displayed high viability after 2 weeks of cultivation on the two nanofiber scaffolds. This suggests that the two nanofiber scaffolds with different degrees of oxidation can provide a desired microenvironment for VSMC-like and EC-like cell growth. Our results are consistent with the finding that MSCs derived from adipose tissue could effectively adhere to and spread on the highly porous pectin-based three-dimensional scaffolds.[51] A similar observation for the attachment and spreading of MSCs on silk hydrogels with different stiffness has been reported by Floren et al.[52]

3.4. Gene Expression of VSMC- or EC-Specific Markers in MSC-Derived VSMCs or ECs.

MSCs have been reported to be able to differentiate into VSMC-like or EC-like cells with the stimulation of TGFβ1 or VEGF, respectively.[53–56] Moreover, it is well recognized that angiogenesis is regulated by mechanobiological factors, such as substrate stiffness and geometrical confinements.[57] Increasing evidence has demonstrated that tissue stiffness and mechanical stimuli are the key cellular microenvironment. To compare the effect of two nanofiber materials with different stiffness on the differentiation of MSCs promoted by TGFβ1 or VEGF into VSMCs or ECs, the mRNA expression levels of three markers specific to VSMCs or ECs were determined by real-time RT-PCR, respectively. As shown in Figure 6, the mRNA expression level of each VSMC-specific marker gene, α-actin, calponin, and smoothelin, was significantly higher in VSMC-like cells cultured on OCP50-ADH nanofiber mats than those on OCP25-ADH nanofiber materials. These findings indicated that the microenvironment provided by OCP50-ADH nanofiber mats was more advantageous for TGFβ1-directed differentiation of MSCs into VSMCs. Similar findings were reported that MSCs grown on silk fibroin biomaterials with a *E*-modulus of 33 kPa and treated with TGF-β1 had high expression levels of mature VSMC markers including calponin-1 and myosin heavy chain 11 (MYH11), compared to the cells cultured on substrates with a *E*-modulus of 6, 20, or 64 kPa.[52,58] Our findings are also consistent with a recent report

that MSCs cultured on stiff substrates had higher expression of VSMC markers α-actin and calponin.[59] With respect to the biophysical mechanisms underlying the fate of stem cells under different culture conditions, increasing evidence has demonstrated that higher substrate stiffness causes stronger cell contractility, which then induces larger cell traction force.[60]

In addition, three EC-specific marker genes, CD31, vWF, and Flk-1 were also quantitatively analyzed at the transcript level by real-time RT-PCR. In contrast to the results of the MSC–VSMC differentiation experiment, the mRNA expression levels of vWF and Flk-1 were downregulated in EC-like cells grown on OCP50-ADH nanofiber mats compared to those grown on OCP25-ADH nanofiber mats (Figure 7). This result was consistent with a previous report that the endothelial phenotype could be significantly increased for MSCs that were cultured on a three-dimensional (3D) nanofiber graft composed of modified poly(ethylene glycol) dimethylacrylate with a low compressive modulus (2 kPa) and treated with VEGF.[58] Moreover, it is reported that a light-emitting diode photopolymerized gelatin methacryloyl hydrogel with an average elastic modulus <2 kPa could enhance vasculature formation.[61] All of these results indicate that the pectin nanofiber scaffolds with different stiffness are able to exert different regulatory effects on MSC differentiation into VSMCs or ECs. Additionally, the effect of substrate rigidity on cell subtype specification and fate decision was also observed on other cell types, such as myofibroblasts, pluripotent stem cells, adipose-derived mesenchymal stem cells, and embryonic stem cells.[62–67] Additional findings reveal the mechanism underlying how MSCs sense local stiffness and make decisions based on the sensed stiffness, in which F-actin serves as a bridge for the mechanotransduction between the ECM and intracellular transcriptional modulation via actin cytoskeleton reorganization.[68]

4. CONCLUSIONS

In summary, the pectin hydrogel nanofibers at 25 and 50% oxidation levels were prepared by periodate oxidation, electrospinning, and ADH-mediated crosslinking of pectin hydrogel nanofibers. The stiffness and hydrophobicity of the obtained pectin hydrogel nanofiber scaffold increased along with the elevation of oxidation and crosslinking levels of the pectin hydrogel. Both the pectin hydrogel nanofiber scaffolds (25 and 50% oxidation) demonstrated high biocompatibility to MSCs that were cultured on the pectin hydrogel nanofiber scaffolds for 14 days. More interestingly, the mechanical cues provided by these two pectin hydrogel nanofiber scaffolds are able to synergistically work with biochemical signals to promote the differentiation of MSCs into distinct phenotypes, i.e., the stiffer pectin hydrogel nanofiber scaffold (50% oxidation level) facilitated MSC–VSMC differentiation, while the softer fiber scaffold induced the MSCs to differentiate into ECs. Altogether, our findings indicate that pectin hydrogel nanofibers possess the capability of providing mechanical cues for inducing MSC differentiation into vascular cells and providing mechanical support for the formation of functioning vessel grafts for vascular tissue engineering.

Supplementary Material

Refer to Web version on PubMed Central for supplementary material.

ACKNOWLEDGMENTS

This work was supported in part by the American Heart Association (15SDG25420001 (Z.H.)), the South Dakota Board of Regents (UP1600205 (Z.H.)), the National Science Foundation/EPSCoR Cooperative Agreement (IIA-1355423), the Fundamental Research Funds for the Central Universities in China (No. 2412019FZ041 (J.H.)), and the National Natural Science Foundation of China (No. 51503027 (J.H.)).

REFERENCES

(1). He W; Nieponice A; Soletti L; Hong Y; Gharaibeh B; Crisan M; Usas A; Peault B; Huard J; Wagner WR; Vorp DA Pericyte-based human tissue engineered vascular grafts. Biomaterials 2010, 31, 8235–8244. [PubMed: 20684982]

(2). L'Heureux N; Dusserre N; Konig G; Victor B; Keire P; Wight TN; Chronos NA; Kyles AE; Gregory CR; Hoyt G; Robbins RC; McAllister TN Human tissue-engineered blood vessels for adult arterial revascularization. Nat. Med 2006, 12, 361–365. [PubMed: 16491087]

(3). L'Heureux N; Dusserre N; Marini A; Garrido S; de la Fuente L; McAllister T Technology insight: the evolution of tissue-engineered vascular grafts–from research to clinical practice. Nat. Clin. Pract. Cardiovasc. Med 2007, 4, 389–395. [PubMed: 17589429]

(4). Meiring M; Khemisi M; Laker L; Dohmen PM; Smit FE Tissue Engineered Small Vessel Conduits - The Anti-Thrombotic Effect of Re-Endothelialization of Decellularized Baboon Arteries: A Preliminary Experimental Study. Med. Sci. Monit. Basic Res 2017, 23, 344–351. [PubMed: 29081492]

(5). Zhang L; Zhou JY; Lu QP; Wei YJ; Hu SS A novel small-diameter vascular graft: In vivo behavior of biodegradable three-layered tubular scaffolds. Biotechnol. Bioeng 2008, 99, 1007–1015. [PubMed: 17705246]

(6). Dahl SL; Koh J; Prabhakar V; Niklason LE Decellularized native and engineered arterial scaffolds for transplantation. Cell Transplant. 2003, 12, 659–666.

(7). Li N; Rickel AP; Sanyour HJ; Hong Z Vessel graft fabricated by the on-site differentiation of human mesenchymal stem cells towards vascular cells on vascular extracellular matrix scaffold under mechanical stimulation in a rotary bioreactor. J. Mater. Chem. B 2019, 7, 2703–2713. [PubMed: 32255003]

(8). Simsa R; Padma AM; Heher P; Hellstrom M; Teuschl A; Jenndahl L; Bergh N; Fogelstrand P Systematic in vitro comparison of decellularization protocols for blood vessels. PLoS One 2018, 13, No. e0209269. [PubMed: 30557395]

(9). Awad NK; Niu H; Ali U; Morsi YS; Lin T Electrospun Fibrous Scaffolds for Small-Diameter Blood Vessels: A Review. Membranes 2018, 8, 15. [PubMed: 29509698]

(10). Hasan A; Memic A; Annabi N; Hossain M; Paul A; Dokmeci MR; Dehghani F; Khademhosseini A Electrospun scaffolds for tissue engineering of vascular grafts. Acta Biomater. 2014, 10, 11–25. [PubMed: 23973391]

(11). Hoshiba T; Lu H; Kawazoe N; Chen G Decellularized matrices for tissue engineering. Expert Opin. Biol. Ther 2010, 10, 1717–1728. [PubMed: 21058932]

(12). Rambøl MH; Hisdal J; Sundhagen JO; Brinchmann JE; Rosales A Recellularization of Decellularized Venous Grafts Using Peripheral Blood: A Critical Evaluation. EBioMedicine 2018, 32, 215–222. [PubMed: 29779699]

(13). Li N; Sanyour H; Remund T; Kelly P; Hong Z Vascular extracellular matrix and fibroblasts-coculture directed differentiation of human mesenchymal stem cells toward smooth muscle-like cells for vascular tissue engineering. Mater. Sci. Eng., C 2018, 93, 61–69.

(14). Negishi J; Hashimoto Y; Yamashita A; Zhang Y; Kimura T; Kishida A; Funamoto S Evaluation of small-diameter vascular grafts reconstructed from decellularized aorta sheets. J. Biomed. Mater. Res., Part A 2017, 105, 1293–1298.

(15). Zhao YL; Zhang S; Zhou JY; Wang JL; Zhen MC; Liu Y; Chen JB; Qi ZQ The development of a tissue-engineered artery using decellularized scaffold and autologous ovine mesenchymal stem cells. Biomaterials 2010, 31, 296–307. [PubMed: 19819544]

(16). Porzionato A; Stocco E; Barbon S; Grandi F; Macchi V; De Caro R Tissue-Engineered Grafts from Human Decellularized Extracellular Matrices: A Systematic Review and Future Perspectives. Int. J. Chem. Biomol. Sci 2018, 19, No. 4117.

(17). Kurobe H; Maxfield MW; Breuer CK; Shinoka T Concise review: tissue-engineered vascular grafts for cardiac surgery: past, present, and future. Stem Cells Transl. Med 2012, 1, 566–571. [PubMed: 23197861]

(18). Song HG; Rumma RT; Ozaki CK; Edelman ER; Chen CS Vascular Tissue Engineering: Progress, Challenges, and Clinical Promise. Cell Stem Cell 2018, 22, 340–354. [PubMed: 29499152]

(19). Henry JJD; Yu J; Wang A; Lee R; Fang J; Li S Engineering the mechanical and biological properties of nanofibrous vascular grafts for in situ vascular tissue engineering. Biofabrication 2017, 9, No. 035007. [PubMed: 28817384]

(20). Wang Z; Qing Q; Chen X; Liu C-J; Luo J-C; Hu J-L; Qin T-W Effects of scaffold surface morphology on cell adhesion and survival rate in vitreous cryopreservation of tenocyte-scaffold constructs. Appl. Surf. Sci 2016, 388, 223–227.

(21). Gelmi A; Cieslar-Pobuda A; de Muinck E; Los M; Rafat M; Jager EW Direct Mechanical Stimulation of Stem Cells: A Beating Electromechanically Active Scaffold for Cardiac Tissue Engineering. Adv. Healthcare Mater 2016, 5, 1471–1480.

(22). Kuang T; Chen F; Chang L; Zhao Y; Fu D; Gong X; Peng X Facile preparation of open-cellular porous poly (l-lactic acid) scaffold by supercritical carbon dioxide foaming for potential tissue engineering applications. Chem. Eng. J 2017, 307, 1017–1025.

(23). Kuang T; Chang L; Chen F; Sheng Y; Fu D; Peng X Facile preparation of lightweight high-strength biodegradable polymer/multi-walled carbon nanotubes nanocomposite foams for electromagnetic interference shielding. Carbon 2016, 105, 305–313.

(24). Ghosal K; Agatemor C; Špitalsky Z; Thomas S; Kny E Electrospinning tissue engineering and wound dressing scaffolds from polymer-titanium dioxide nanocomposites. Chem. Eng. J 2019, 358, 1262–1278.

(25). Lee E-S; Lei D; Devarayan K; Kim B-S High strength poly(vinyl alcohol)/poly(acrylic acid) cross-linked nanofibrous hybrid composites incorporating nanohybrid POSS. Compos. Sci. Technol 2015, 110, 111–117.

(26). Li S; Sengupta D; Chien S Vascular tissue engineering: from in vitro to in situ. Wiley Interdiscip. Rev.: Syst. Biol. Med 2014, 6, 61–76.

(27). Kurpinski KT; Stephenson JT; Janairo RR; Lee H; Li S The effect of fiber alignment and heparin coating on cell infiltration into nanofibrous PLLA scaffolds. Biomaterials 2010, 31, 3536–3542. [PubMed: 20122725]

(28). Maxwell EG; Belshaw NJ; Waldron KW; Morris VJ Pectin – An emerging new bioactive food polysaccharide. Trends Food Sci. Technol 2012, 24, 64–73.

(29). Almeida EAMS; Facchi SP; Martins AF; Nocchi S; Schuquel ITA; Nakamura CV; Rubira AF; Muniz EC Synthesis and characterization of pectin derivative with antitumor property against Caco-2 colon cancer cells. Carbohydr. Polym 2015, 115, 139–145. [PubMed: 25439878]

(30). Ho GTT; Ahmed A; Zou Y-F; Aslaksen T; Wangensteen H; Barsett H Structure–activity relationship of immunomodulating pectins from elderberries. Carbohydr. Polym 2015, 125, 314–322. [PubMed: 25857988]

(31). Popov SV; Ovodova RG; Golovchenko VV; Khramova DS; Markov PA; Smirnov VV; Shashkov AS; Ovodov YS Pectic polysaccharides of the fresh plum Prunus domestica L. isolated with a simulated gastric fluid and their anti-inflammatory and antioxidant activities. Food Chem. 2014, 143, 106–113. [PubMed: 24054219]

(32). Liu Y; Zheng D; Ma Y; Dai J; Li C; Xiao S; Liu K; Liu J; Wang L; Lei J; He J Self-Assembled Nanoparticles Platform Based on Pectin-Dihydroartemisinin Conjugates for Codelivery of Anticancer Drugs. ACS Biomater. Sci. Eng 2018, 4, 1641–1650. [PubMed: 33445320]

(33). Jung J; Arnold RD; Wicker L Pectin and charge modified pectin hydrogel beads as a colon-targeted drug delivery carrier. Colloids Surf., B 2013, 104, 116–121.

Health Research Alliance Author Manuscript

(34). Chen S; Cui S; Zhang H; Pei X; Hu J; Zhou Y; Liu Y Cross-Linked Pectin Nanofibers with Enhanced Cell Adhesion. Biomacromolecules 2018, 19, 490–498. [PubMed: 29257671]

(35). Assaf SM; Abul-Haija YM; Fares MM Versatile Pectin Grafted Poly (N-isopropylacrylamide); Modulated Targeted Drug Release. J. Macromol. Sci., Part A: Pure Appl. Chem 2011, 48, 493–502.

(36). Munarin F; Guerreiro SG; Grellier MA; Tanzi MC; Barbosa MA; Petrini P; Granja PL Pectin-Based Injectable Biomaterials for Bone Tissue Engineering. Biomacromolecules 2011, 12, 568–577. [PubMed: 21302960]

(37). Birch NP; Barney LE; Pandres E; Peyton SR; Schiffman JD Thermal-Responsive Behavior of a Cell Compatible Chitosan/Pectin Hydrogel. Biomacromolecules 2015, 16, 1837–1843. [PubMed: 25932898]

(38). Barron V; Lyons E; Stenson-Cox C; McHugh PE; Pandit A Bioreactors for cardiovascular cell and tissue growth: a review. Ann. Biomed. Eng 2003, 31, 1017–1030. [PubMed: 14582605]

(39). Heyligers JM; Arts CH; Verhagen HJ; de Groot PG; Moll FL Improving small-diameter vascular grafts: from the application of an endothelial cell lining to the construction of a tissue-engineered blood vessel. Ann. Vasc. Surg 2005, 19, 448–456. [PubMed: 15864472]

(40). Mitchell SL; Niklason LE Requirements for growing tissue-engineered vascular grafts. Cardiovasc. Pathol 2003, 12, 59–64. [PubMed: 12684159]

(41). Gluck JM; Delman C; Chyu J; MacLellan WR; Shemin RJ; Heydarkhan-Hagvall S Microenvironment influences vascular differentiation of murine cardiovascular progenitor cells. J. Biomed. Mater. Res., Part B 2014, 102, 1730–1739.

(42). Hou L; Kim JJ; Wanjare M; Patlolla B; Coller J; Natu V; Hastie TJ; Huang NF Combinatorial Extracellular Matrix Microenvironments for Probing Endothelial Differentiation of Human Pluripotent Stem Cells. Sci. Rep 2017, 7, No. 6551. [PubMed: 28747756]

(43). Wang CH; Wang TM; Young TH; Lai YK; Yen ML The critical role of ECM proteins within the human MSC niche in endothelial differentiation. Biomaterials 2013, 34, 4223–4234. [PubMed: 23489927]

(44). Wingate K; Bonani W; Tan Y; Bryant SJ; Tan W Compressive elasticity of three-dimensional nanofiber matrix directs mesenchymal stem cell differentiation to vascular cells with endothelial or smooth muscle cell markers. Acta Biomater. 2012, 8, 1440–1449. [PubMed: 22266031]

(45). Zhang H; Cui S; Lv H; Pei X; Gao M; Chen S; Hu J; Zhou Y; Liu Y A crosslinking strategy to make neutral polysaccharide nanofibers robust and biocompatible: With konjac glucomannan as an example. Carbohydr. Polym 2019, 215, 130–136. [PubMed: 30981337]

(46). Cui S; Yao B; Sun X; Hu J; Zhou Y; Liu Y Reducing the content of carrier polymer in pectin nanofibers by electrospinning at low loading followed with selective washing. Mater. Sci. Eng., C 2016, 59, 885–893.

(47). Sanyour H; Childs J; Meininger GA; Hong ZK Spontaneous oscillation in cell adhesion and stiffness measured using atomic force microscopy. Sci. Rep 2018, 8, No. 2899. [PubMed: 29440673]

(48). Sanyour HJ; Li N; Rickel AP; Childs JD; Kinser CN; Hong ZK Membrane cholesterol and substrate stiffness co-ordinate to induce the remodelling of the cytoskeleton and the alteration in the biomechanics of vascular smooth muscle cells. Cardiovasc. Res 2019, 115, 1369–1380. [PubMed: 30395154]

(49). Cui S; Yao B; Gao M; Sun X; Gou D; Hu J; Zhou Y; Liu Y Effects of pectin structure and crosslinking method on the properties of crosslinked pectin nanofibers. Carbohydr. Polym 2017, 157, 766–774. [PubMed: 27987989]

(50). Parmar N; Ahmadi R; Day RM A Novel Method for Differentiation of Human Mesenchymal Stem Cells into Smooth Muscle-Like Cells on Clinically Deliverable Thermally Induced Phase Separation Microspheres. Tissue Eng., Part C 2015, 21, 404–412.

(51). Kulikouskaya V; Kraskouski A; Hileuskaya K; Zhura A; Tratsyak S; Agabekov V Fabrication and characterization of pectin-based three-dimensional porous scaffolds suitable for treatment of peritoneal adhesions. J. Biomed. Mater. Res., Part A 2019, 107, 1814–1823.

(52). Floren M; Bonani W; Dharmarajan A; Motta A; Migliaresi C; Tan W Human mesenchymal stem cells cultured on silk hydrogels with variable stiffness and growth factor differentiate into mature smooth muscle cell phenotype. Acta Biomater. 2016, 31, 156–166. [PubMed: 26621695]

(53). Parvizi M; Bolhuis-Versteeg LAM; Poot AA; Harmsen MC Efficient generation of smooth muscle cells from adipose-derived stromal cells by 3D mechanical stimulation can substitute the use of growth factors in vascular tissue engineering. Biotechnol. J 2016, 11, 932–944. [PubMed: 26989865]

(54). Wang CG; Li Y; Yang M; Zou YH; Liu HH; Liang ZY; Yin Y; Niu GC; Yan ZG; Zhang BH Efficient Differentiation of Bone Marrow Mesenchymal Stem Cells into Endothelial Cells in Vitro. Eur. J. Vasc. Endovasc. Surg 2018, 55, 257–265. [PubMed: 29208350]

(55). Chen MY; Lie PC; Li ZL; Wei X Endothelial differentiation of Wharton's jelly-derived mesenchymal stem cells in comparison with bone marrow-derived mesenchymal stem cells. Exp. Hematol 2009, 37, 629–640. [PubMed: 19375653]

(56). Lu W; Su L; Yu ZZ; Zhang SL; Miao JY The New Role of CD163 in the Differentiation of Bone Marrow Stromal Cells into Vascular Endothelial-Like Cells. Stem Cells Int. 2016, 2016, No. 2539781. [PubMed: 26880943]

(57). Chen ZW; Zhao RG Engineered Tissue Development in Biofabricated 3D Geometrical Confinement-A Review. ACS Biomater. Sci. Eng 2019, 5, 3688–3702. [PubMed: 33405885]

(58). Henderson K; Sligar AD; Le VP; Lee J; Baker AB Biomechanical Regulation of Mesenchymal Stem Cells for Cardiovascular Tissue Engineering. Adv. Healthcare Mater 2017, 6, No. 1700556.

(59). Park JS; Chu JS; Tsou AD; Diop R; Tang ZY; Wang AJ; Li S The effect of matrix stiffness on the differentiation of mesenchymal stem cells in response to TGF-beta. Biomaterials 2011, 32, 3921–3930. [PubMed: 21397942]

(60). Yu Y; Liu SS; Wu XA; Yu Z; Xu YS; Zhao WJ; Zayodnik I; Zheng JP; Li C; Zhao HC Mechanism of Stiff Substrates up-Regulate Cultured Neuronal Network Activity. ACS Biomater. Sci. Eng 2019, 5, 3475–3482. [PubMed: 33405731]

(61). Monteiro N; He WT; Franca CM; Athirasala A; Bertassoni LE Engineering Microvascular Networks in LED Light-Cured Cell-Laden Hydrogels. ACS Biomater. Sci. Eng 2018, 4, 2563–2570. [PubMed: 33435119]

(62). Davidson MD; Song KH; Lee MH; Llewellyn J; Du Y; Baker BM; Wells RG; Burdick JA Engineered Fibrous Networks To Investigate the Influence of Fiber Mechanics on Myofibroblast Differentiation. ACS Biomater. Sci. Eng 2019, 5, 3899–3908. [PubMed: 33438429]

(63). Sun YB; Yong KMA; Villa-Diaz LG; Zhang XL; Chen WQ; Philson R; Weng SN; Xu HX; Krebsbach PH; Fu JP Hippo/YAP-mediated rigidity-dependent motor neuron differentiation of human pluripotent stem cells. Nat. Mater 2014, 13, 599–604. [PubMed: 24728461]

(64). Sthanam LK; Saxena N; Mistari VK; Roy T; Jadhav SR; Sen S Initial Priming on Soft Substrates Enhances Subsequent Topography-Induced Neuronal Differentiation in ESCs but Not in MSCs. ACS Biomater. Sci. Eng 2019, 5, 180–192. [PubMed: 33405870]

(65). Fu JY; Chuah YJ; Liu J; Tan SY; Wang DA Respective Effects of Gelatin-Coated Polydimethylsiloxane (PDMS) Substrates on Self-renewal and Cardiac Differentiation of Induced Pluripotent Stem Cells (iPSCs). ACS Biomater. Sci. Eng 2018, 4, 4321–4330. [PubMed: 33418827]

(66). Mittal N; Tasnim F; Yue C; Qu YH; Phan D; Choudhury Y; Tan MH; Yu H Substrate Stiffness Modulates the Maturation of Human Pluripotent Stem-Cell-Derived Hepatocytes. ACS Biomater. Sci. Eng 2016, 2, 1649–1657. [PubMed: 33440598]

(67). Banks JM; Harley BAC; Bailey RC Tunable, Photoreactive Hydrogel System To Probe Synergies between Mechanical and Biomolecular Cues on Adipose-Derived Mesenchymal Stem Cell Differentiation. ACS Biomater. Sci. Eng 2015, 1, 718–725. [PubMed: 33435093]

(68). Fan YL; Zhao HC; Li B; Zhao ZL; Feng XQ Mechanical Roles of F-Actin in the Differentiation of Stem Cells: A Review. ACS Biomater. Sci. Eng 2019, 5, 3788–3801. [PubMed: 33438419]

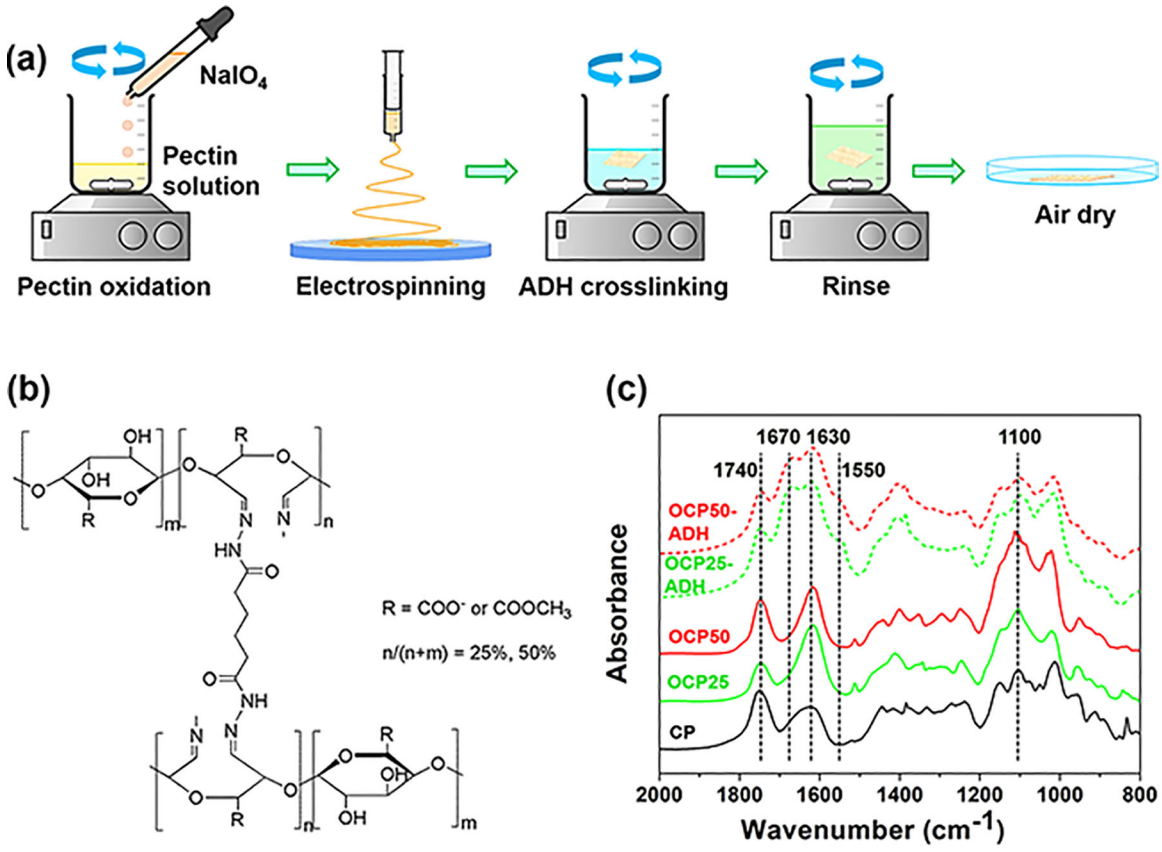

Figure 1.

(a) Schematic of the preparation of pectin hydrogel nanofiber scaffolds; (b) schematic illustration of the chemical structure of the pectin hydrogel nanofibers; (c) FTIR spectra of pristine, oxidized pectin, and obtained crosslinked pectin hydrogel nanofibers.

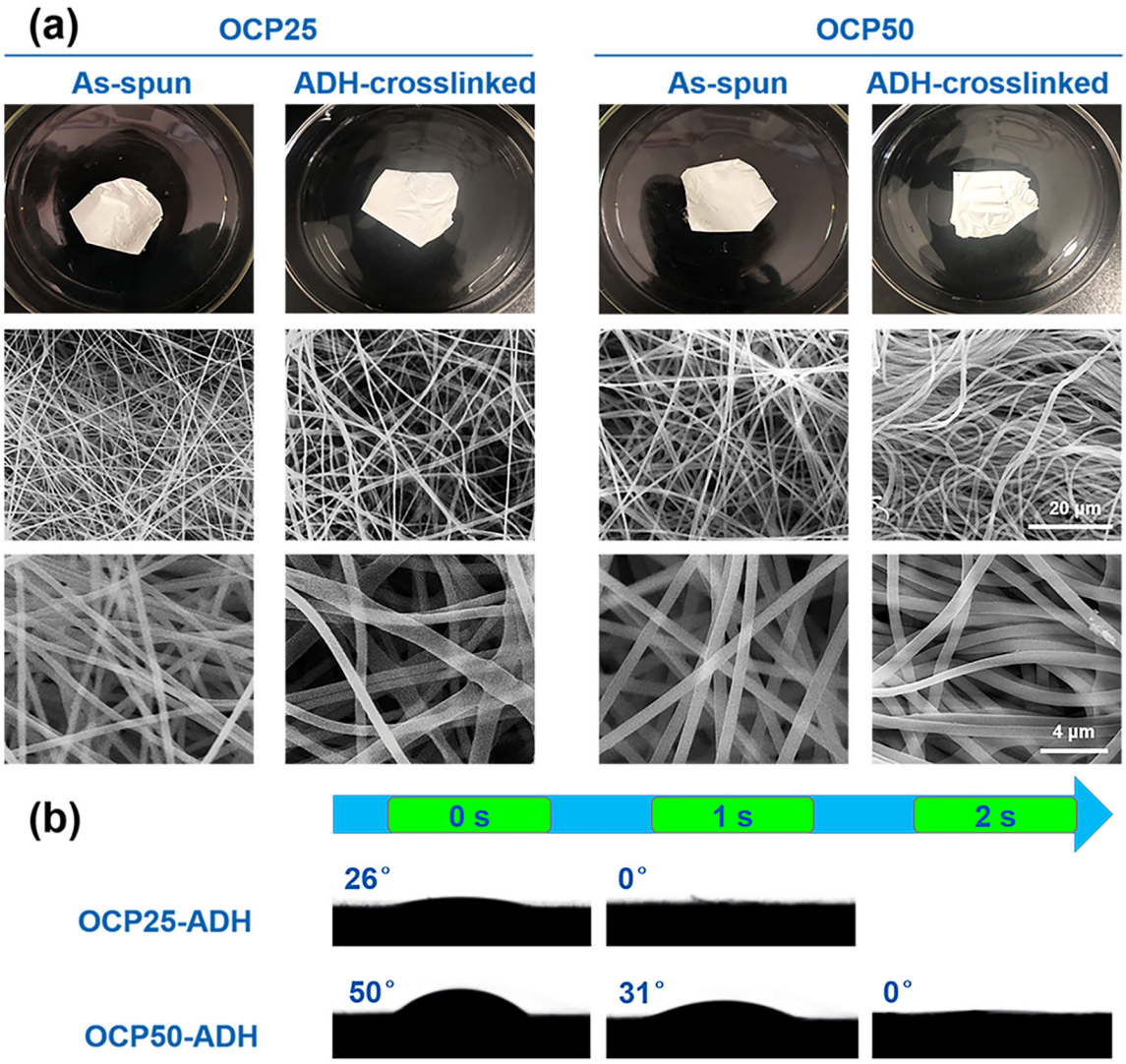

Figure 2.

(a) SEM images of the as-spun and ADH-crosslinked OCP nanofibers. No significant difference was observed between the OCP25 and OCP50 nanofibers. ADH crosslinking did not change the fiber morphology. (b) Water absorption process of the pectin hydrogel nanofiber scaffolds. A higher oxidation level leads to lower water wettability of the pectin hydrogel nanofiber scaffolds.

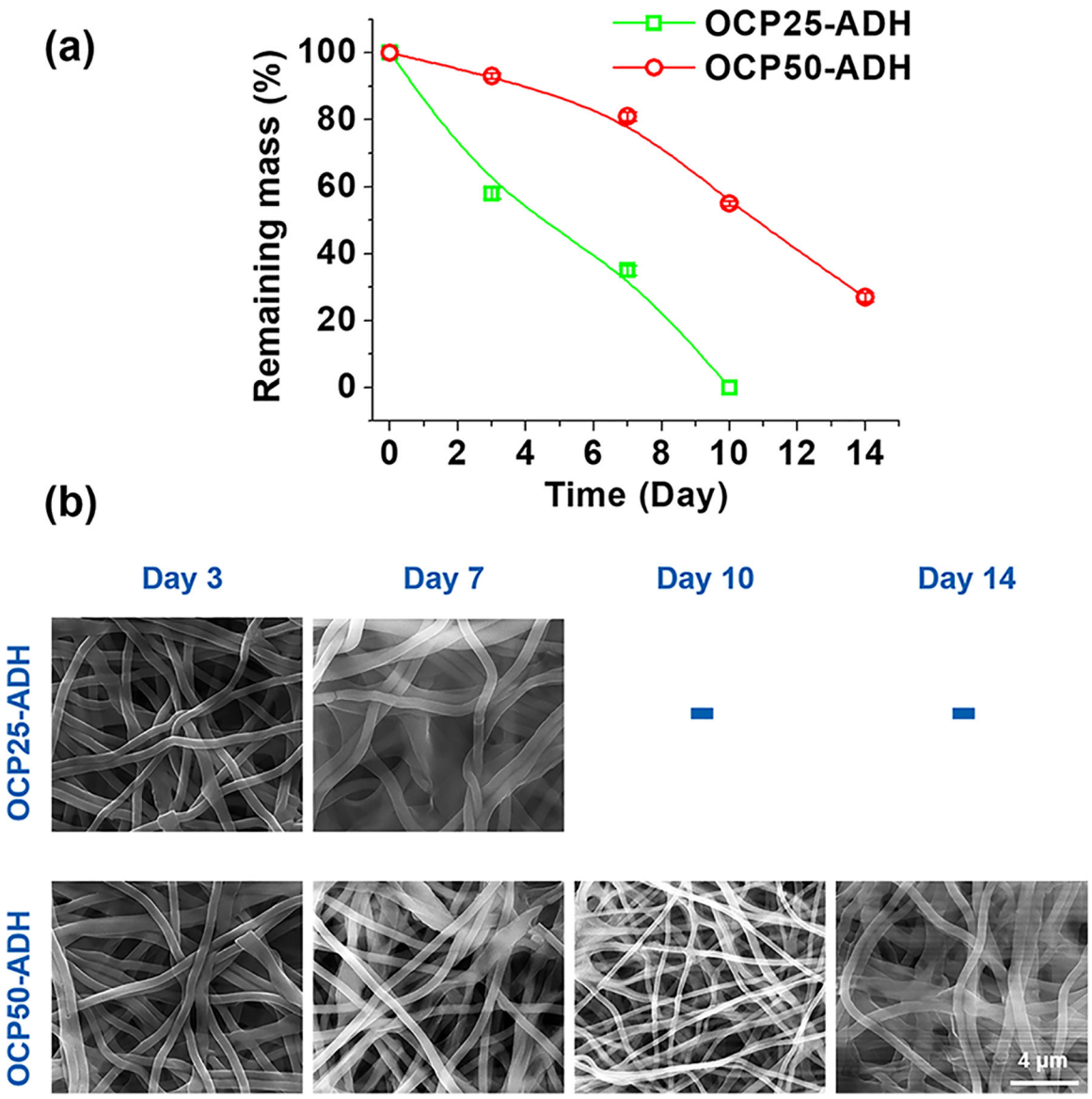

Figure 3.

Alteration in mass (a) and morphology (b) of pectin hydrogel nanofiber scaffolds that were incubated in SBF for various periods of time. Prior to weighing, all samples were washed six times with distilled water to remove the buffer (inorganic salts) retained in the nanofiber mats, rinsed with ethanol and chloroform, and air dried for 24 h.

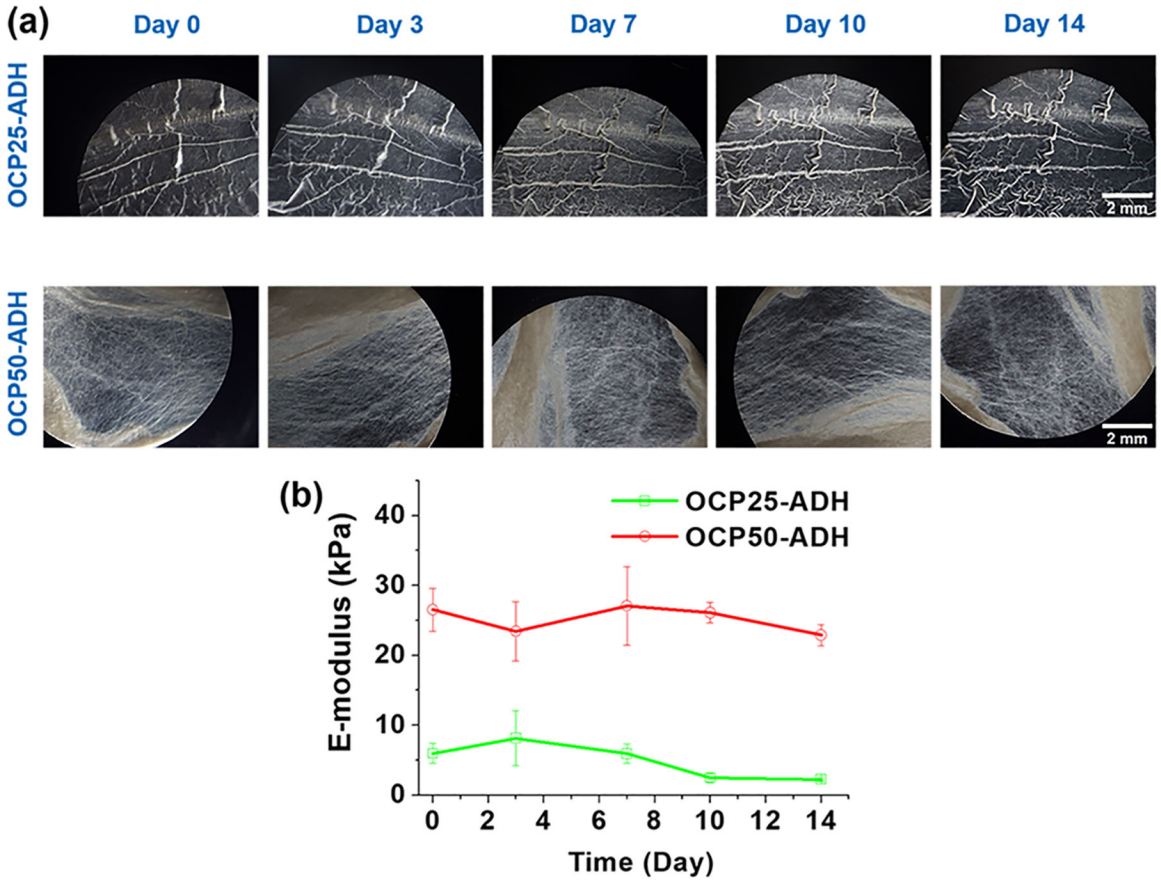

Figure 4.

(a) Morphology of pectin nanofiber mats after incubation for different time points in MSC culture medium. No significant morphology changes were observed for both OCP25-ADH and OCP50-ADH after 14 days incubation. (b) *E*-moduli of the pectin hydrogel nanofibers were monitored using AFM at different time points. The *E*-moduli of OCP25-ADH started to decrease after 10 days incubation, while the OCP50-ADH nanofiber scaffold exhibited no significant change in *E*-modulus.

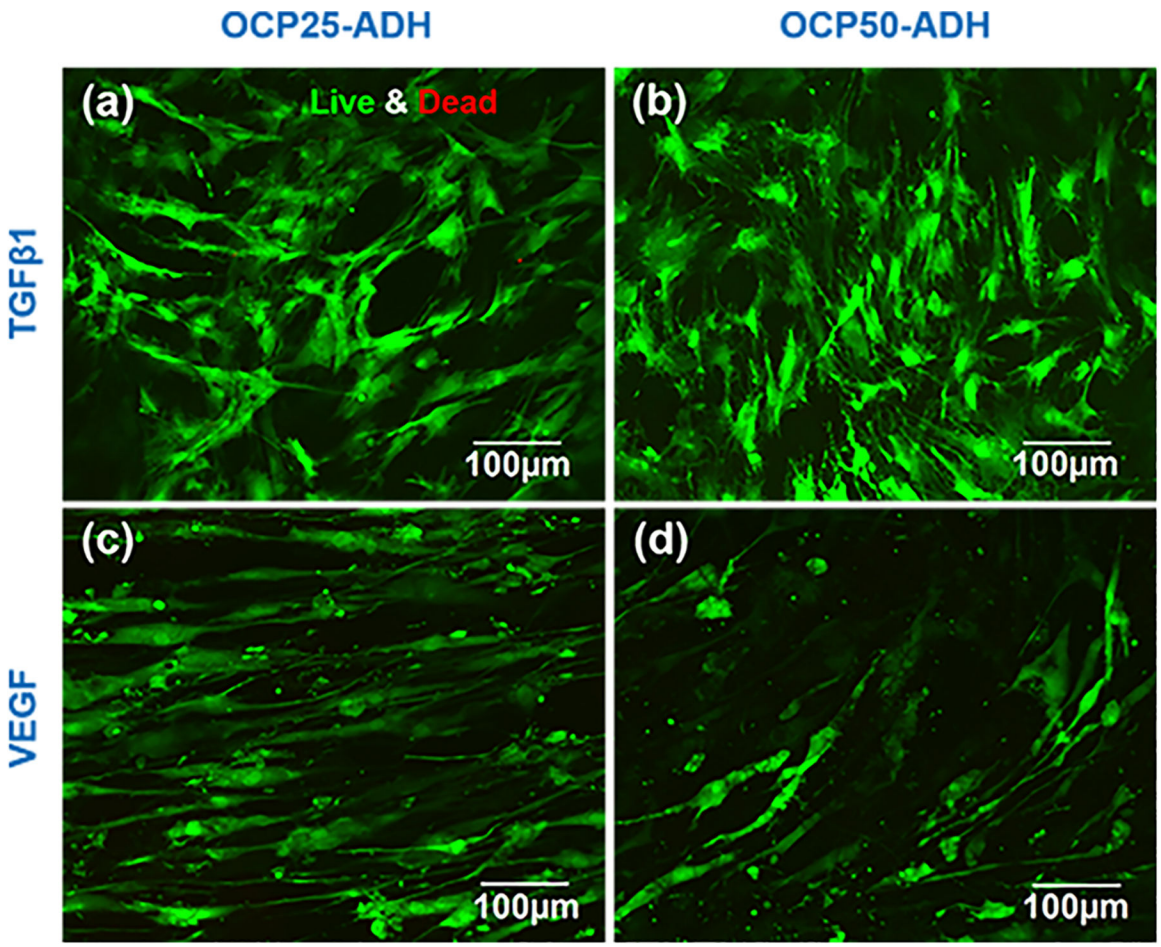

Figure 5.

Live/Dead staining showed MSCs cultured on the pectin nanofiber scaffolds with different oxidation levels for 14 days. MSCs were cultured with TGFβ1 medium on (a) OCP25-ADH and (b) OCP50-ADH scaffolds for 14 days, respectively. MSCs were cultured with VEGF medium on (c) OCP25-ADH and (d) OCP50-ADH scaffolds for 14 days, respectively. Both the pectin nanofiber mats exhibited high compatibility for MSC growth.

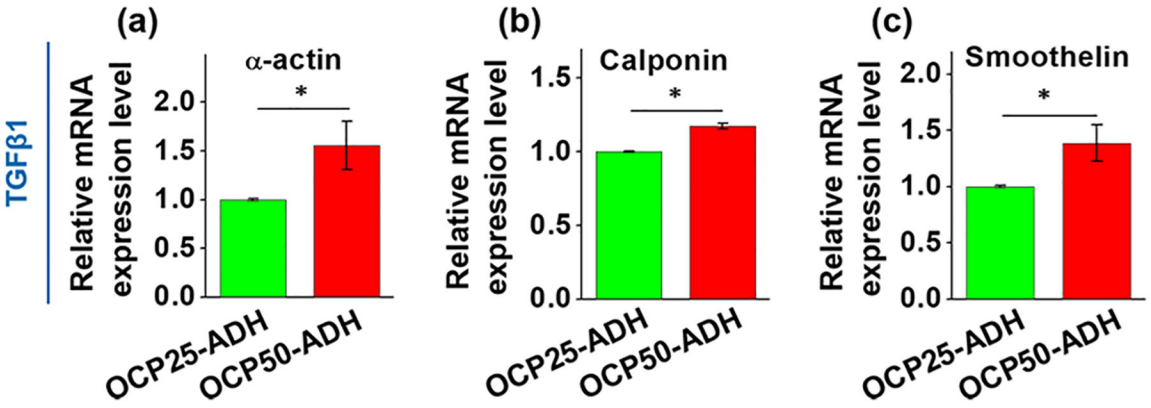

Figure 6.

Real-time RT-PCR result for the gene expression of VSMC-specific marker genes, (a) α-actin, (b) calponin, and (c) smoothelin. The increase in the oxidation level of the pectin hydrogel nanofiber mat enhanced the expression of all three VSMC-specific marker genes ($p < 0.05$). $n = 6$.

Health Research Alliance Author Manuscript

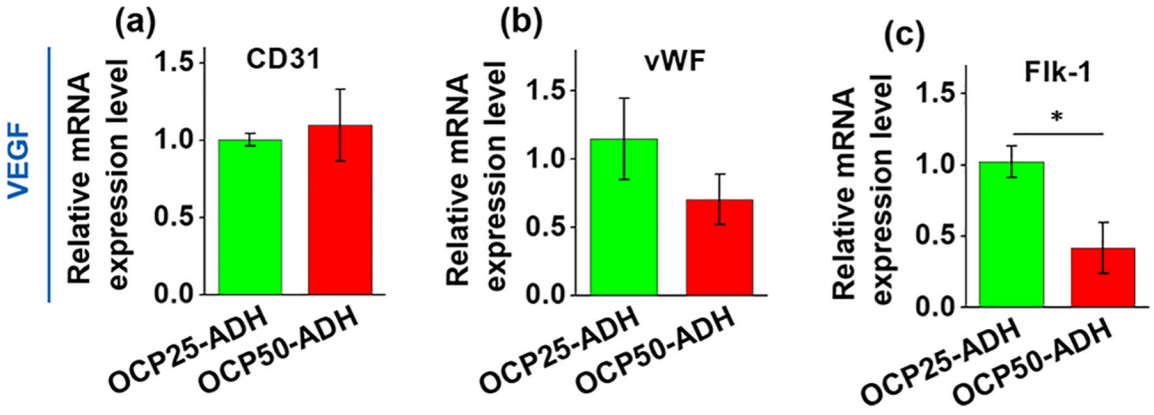

Figure 7.

Real-time RT-PCR result for the gene expression of EC-specific marker genes, (a) CD31, (b) vWF, and (c) Flk-1. The increase in the oxidation level of the pectin hydrogel nanofiber mat attenuated the expression of EC-specific marker genes vWF ($p > 0.05$) and Flk-1 ($p < 0.05$). $n = 6$.